© Photos: DOI: 10.2516/ogst/2013139, IFPEN, X

Dossier

This paper is a part of the hereunder thematic dossier published in OGST Journal, Vol. 69, No. 1, pp. 3-188 and available online here

Cet article fait partie du dossier thématique ci-dessous publié dans la revue OGST, Vol. 69, n°1, pp. 3-188 et téléchargeable ici

DOSSIER Edited by/Sous la direction de : **C. Angelberger**

IFP Energies nouvelles International Conference / Les Rencontres Scientifiques d'IFP Energies nouvelles

LES4ICE 2012 - Large Eddy Simulation for Internal Combustion Engine Flows

LES4ICE 2012 - La simulation aux grandes échelles pour les écoulements dans les moteurs à combustion interne

Oil & Gas Science and Technology – Rev. IFP Energies nouvelles, Vol. 69 (2014), No. 1, pp. 3-188

Oil & Gas Science and Technology – Rev. IFP Energies nouvelles, Vol. 69 (2014), No. 1, pp. 155-165

DOI: 10.2516/ogst/2013139

IFP Energies nouvelles International Conference
Rencontres Scientifiques d'IFP Energies nouvelles

LES4ICE 2012 - Large Eddy Simulation for Internal Combustion Engine Flows
LES4ICE 2012 - La simulation aux grandes échelles pour les écoulements dans les moteurs à combustion interne

Large-Eddy Simulation of Diesel Spray Combustion with Exhaust Gas Recirculation

J. Tillou[1,2], J.-B. Michel[1], C. Angelberger[1]*, C. Bekdemir[3] and D. Veynante[2]

[1] *IFP Energies nouvelles, 1-4 avenue de Bois-Préau, 92852 Rueil-Malmaison Cedex - France*
[2] *École Centrale Paris, Grande Voie des Vignes, 92295 Châtenay-Malabry Cedex - France*
[3] *Mechanical Engineering, Eindhoven University of Technology, Den Dolech 2, 5612 AZ Eindhoven - The Netherlands*
e-mail: julien.tillou@ifpen.fr - jean-baptiste.michel@ifpen.fr - christian.angelberger@ifpen.fr - c.bekdemir@tue.nl denis.veynante@ecp.fr

* Corresponding author

Résumé — **Simulation aux grandes échelles de la combustion d'un spray Diesel pour différents taux d'EGR** — La simulation aux grandes échelles (LES Large Eddy Simulations) de la combustion est appliquée à l'expérience du spray H réalisée dans le cadre de l'ECN (*Engine Combustion Network*). Le modèle ADF-PCM, dont le principe repose sur la résolution de flammelettes approchées, a été adapté à la LES de façon à simuler la combustion dans cette étude. Les effets chimiques complexes peuvent ainsi être pris en compte. La résolution de la phase liquide est réalisée *via* une approche mésoscopique Eulérienne couplée au modèle DITurBC pour l'injection.

La structure de la combustion résultant du jet de carburant est étudiée puis comparée avec les observations expérimentales. Les résultats obtenus pour de faibles taux de gaz recirculants (EGR : *Exhaust Gas Recirculation*) reproduisent de façon très fidèle ceux de l'expérience. Bien que l'effet de l'ajout d'EGR soit qualitativement reproduit, les prédictions obtenues par la LES se détériorent avec le taux d'EGR. L'utilisation d'un schéma cinétique validé uniquement pour de faibles taux d'EGR est une explication possible de la mauvaise reproduction des effets de forts taux d'EGR.

Abstract — ***Large-Eddy Simulation of Diesel Spray Combustion with Exhaust Gas Recirculation*** — *A Large-Eddy Simulation (LES) study of the transient combustion in the spray H experiment investigated in the frame of the Engine Combustion Network (ECN) is presented. Combustion is modeled using a LES formulation of the ADF-PCM approach, the principle of which is to tabulate approximated diffusion flames based on the flamelet equation to account for complex chemical effects. The liquid phase is resolved with an Eulerian mesoscopic approach coupled with the DITurBC model for the injection.*

The structure of the combustion resulting from the n-heptane liquid fuel jet is investigated and compared to the literature. A very good reproduction of experimental findings by the presented LES approach is reported for small EGR rates. Albeit the qualitative effect of increasing the EGR rate is captured, the quantitative quality of the LES predictions deteriorates with increasing EGR rate. One possible explanation for this poor reproduction of EGR effects might be related to the fact that the used semi-detailed scheme was not validated for high EGR rates.

INTRODUCTION

A detailed understanding of Diesel engine combustion is critical to improve engine efficiency while reducing pollutant emissions. To study Diesel engine combustion, constant volume chambers are often used [1, 2]. They allow studying transient liquid jet combustion under conditions representative of Diesel engines, without the complexity inherent to such devices.

The simulation of constant volume chambers is still a challenge requiring to model spray formation, liquid evaporation, auto-ignition and flame stabilisation. Three major parameters are used to characterise the Diesel spray combustion: the Heat Release Rate (HRR), the auto-igniting delay and the Lift-Off Length (LOL) [1, 3, 4].

An important literature already exists concerning Reynolds average Navier Stockes (RANS) simulation of the spray H experiment. Gopalakrishnan and Abrahams [5] performed Representative Interactive Flamelet (RIF) [6] computations comparing heat release rate and auto-ignition localisation. Tap and Veynante [7] developed a generalised surface density modeling approach assessed on lift-off length for several injector diameters and ambient densities. Lift-off length predictions based on the strain rate have been performed by Venugopal and Abraham [4] for several chamber densities, temperatures, and oxygen concentrations. Azimov *et al*. [8] used the ECFM3Z (3-Zones Extended Coherent Flame Model) [9] combustion model to predict flame LOL and HRR. Novella *et al*. [3] compared different chemical schemes assuming homogeneous combustion at the filter size. The chemistry was assessed on LOL, auto-ignition delay and HRR for different temperatures and oxygen concentrations.

Contrary to RANS, LES takes into account local, instantaneous, spatially filtered flow phenomena, resolving the largest flow scales and modeling only the effects of the smallest ones. It thus appears as having a good potential for addressing unsteady and highly stratified flow found in Diesel combustion. While the literature proposes several studies of LES of Diesel engines [10, 11], very few has been published to date on LES of liquid spray combustion in constant volume chambers. Bekdemir *et al*. [12] used a FGM (Flamelet Generated Manifold) model [13] adapted to LES to predict LOL and auto-ignition delays and compare with experimental findings for Spray H.

In the present paper, the ADF-PCM (Approximated Diffusion Flame - Presumed Conditional Moment) turbulent combustion model initially developed for partially premixed and non-premixed combustion in the RANS context by Michel *et al*. [14-16] is adapted to LES. It is combined with an Eulerian mesoscopic formalism describing the liquid jet and applied to the LES of the Spray H, experimentally studied by Sandia in the context of ECN [17-19]. It proposes a wide range of parametric variations and especially of EGR rates (Exhaust Gas Recirculation).

Section 1 presents the ADF-PCM model and its integration to the AVBP LES solver [20]. Section 2 then describes the numerical set-up and the different cases investigated. Finally, Section 3 compares the obtained results with experimental findings with emphasis on the reproduction of the impact of EGR rate on combustion characteristics.

1 THE ADF-PCM MODEL

The ADF-PCM model [14-16] tabulates auto-igniting approximated diffusion flames. These flames possess the advantage to be computed in a very short time, even for detailed chemical schemes. Indeed, unlike the computation of laminar diffusion flames which requires the resolution of the flamelet equation [21] for each species of the chemical scheme, the ADF approach resolves the flamelet equation only for the progress variable and extracts the chemical source term of this equation from a Homogeneous Reactor (HR) look-up table.

1.1 Approximated Diffusion Flame

The ADF approach consists in resolving the flamelet equation [21] for a progress variable Y_c:

$$\frac{\partial Y_c^{flam}}{\partial t} = \chi \frac{\partial^2 Y_c^{flam}}{\partial Z^2} + \dot{\omega}_{Y_c^{flam}} \tag{1}$$

where Y_c^{flam} indicates the progress variable transported by the flamelet equation and Z denotes the mixture fraction. The progress variable Y_c is defined as proposed by [22]:

$$Y_c = Y_{CO} + Y_{CO_2} \tag{2}$$

The scalar dissipation rate χ is defined as:

$$\chi = D\left|\frac{\partial Z}{\partial x}\right|^2 \tag{3}$$

with D the mass diffusion coefficient. This quantity measures the rate of mixing and can be expressed, considering a counterflow diffusion flame with constant density, as a function of the mixture fraction Z and the strain rate a [23]:

$$\chi(Z,a) = \frac{a}{2\pi}\exp\left(-2\left[\mathrm{erf}^{-1}(1-2Z)\right]^2\right) = aF(Z) \quad (4)$$

with erf^{-1} the inverse error function. The source term $\dot{\omega}_{Y_c^{flam}}$ is extracted from a previously built look-up table based on Homogeneous Reactors (HR) at constant pressure. Each HR is initialised for different initial temperatures T_u and mixture fractions Z. In the present case, the pressure is set to the experimental value of 42.25 bar. The set of initial conditions is chosen in order to map all the conditions that can be encountered during the simulation. This look-up table stores the species mass fraction Y_i and the reaction rate $\dot{\omega}_{Y_c}$ as functions of discrete values of Z, T_u and c, the normalized progress variable defined as:

$$c = \frac{Y_c}{Y_c^{eq}} \quad (5)$$

where the *eq* superscript denotes the thermodynamical equilibrium at constant pressure and enthalpy. The reaction rate of the flamelet (*Eq. 1*) is extracted from the HR look-up table following:

$$\dot{\omega}_{Y_c}^{flam} = \dot{\omega}_{Y_c}^{HR}\left(c^{flam}, Z, T_u(Z)\right) \quad (6)$$

with c^{flam} the normalized progress variable reconstructed with Y_c^{flam} using Equation (5) and with $T_u(Z)$ the fresh gas temperature stratification considered as a linear function of the mixture fraction for the approximated diffusion flame. Figure 1 presents a schematic view of the ADF approach.

Equation (1) is solved for different values of the strain rate a and the temperature stratification $T_u(Z)$. This allows building an intermediate ADF look-up table containing the species mass fractions extracted from the HR look-up table with the progress variable from the flamelet equation:

$$Y_i^{ADF}(t,Z,T_u(Z),a) = Y_i^{HR}(c^{flam},Z,T_u(Z)) \quad (7)$$

This look-up table is completed by the flamelet progress variable variation rate following:

$$\dot{\omega}_{Y_c}^{ADF}(t,Z,T_u(Z),a) = \frac{\partial Y_c^{flam}}{\partial t}(c^{flam},Z,T_u(Z)) \quad (8)$$

The semi-detailed chemical scheme of Seiser *et al.* [24] containing 1 540 reactions among 160 species is chosen for the HR computation. It has been especially validated on counterflow diffusion flame configurations at 1 bar and on ignition delays up to 100 bar. This mechanism has been used in prior studies of the spray H experiment [4, 5] and is recommended by the ECN group.

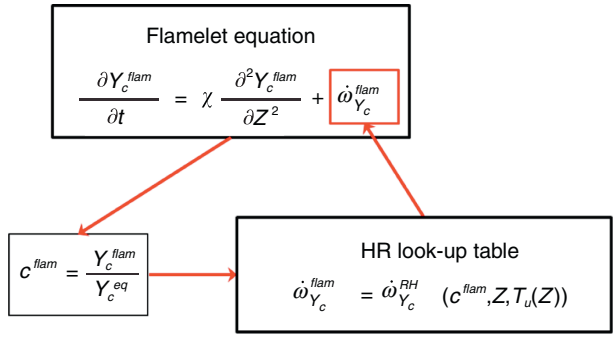

Figure 1

Scheme of the ADF approach. The flamelet equation is resolved for Y_c^{flam} and the source term of this equation is extracted from the HR look-up table.

1.2 The ADF-PCM Look-Up Table

In order to take the subgrid scale mixture stratification into account, the species mass fractions and reaction rates of the ADF look-up table are finally integrated using a presumed Probability Density Function (PDF) which is assumed to be a β function. It is parameterised by the local mixture fraction Z, the filtered mixture fraction $\tilde{Z}$ and its segregation factor S_z. This PDF is denoted as $P(Z)$ for the sake of clarity. It results in the ADF-PCM look-up table containing all the species transported in the CFD code, as well as the reaction rate of the filtered progress variable:

$$\tilde{Y}_i^{ADF-PCM}\left(t,\tilde{Z},S_z,\tilde{T}_a,\tilde{T}_f,a\right) = \int_{Z=0}^{Z_s} Y_i^{ADF}(t,Z,\tilde{T}_u(Z),a)\tilde{P}(Z)dZ \quad (9)$$

$$\tilde{\dot{\omega}}_{Y_c}^{ADF-PCM}\left(t,\tilde{Z},S_z,\tilde{T}_a,\tilde{T}_f,a\right) = \int_{Z=0}^{Zs} \dot{\omega}_{Y_c}^{ADF}(t,Z,\tilde{T}_u(Z),a)\tilde{P}(Z)dZ \quad (10)$$

As the temperature stratification $T_u(Z)$ of the flamelet is considered linear, it is characterised by only two temperatures: the air temperature $T_a(Z=0)$ and the fuel temperature $T_f(Z=Z_s)$. Z_s denotes the mixture fraction saturation value set equal to 0.5. The mixture fraction segregation factor S_z is defined as:

$$S_z = \frac{Z_v}{\tilde{Z}(Z_s - \tilde{Z})} \quad (11)$$

where Z_v is the mixture fraction variance. Finally, the filtered progress variable $\tilde{c}$ is used instead of the time to

parametrise the look-up table. It is computed using Equation (5) with $\tilde{Y}_{CO}^{ADF-PCM}$ and $\tilde{Y}_{CO_2}^{ADF-PCM}$ (*Eq. 9*). Finally, the look-up table is parameterised as a function of $\tilde{c}$, $\tilde{Z}$, S_z, $\tilde{T}_a$, $\tilde{T}_f$ and a.

1.3 LES Transport Equations for the ADF-PCM Approach

The implementation of the ADF-PCM model in the compressible LES flow solver AVBP [20] requires to add some additional transport equations.

1.3.1 Filtered Mixture Fraction

The mixture fraction Z is defined as a fuel tracer, as already performed in several past studies about Diesel combustion modeling [9]. By definition, this tracer is convected and diffused exactly as the species it considers but it is not consumed during the combustion. It varies from 0 for pure air to 1 for pure fuel. The filtered mixture fraction transport equation writes:

$$\frac{\partial \bar{\rho}\tilde{Z}}{\partial t} + \frac{\partial}{\partial x_j}\left(\bar{\rho}\tilde{u}_j\tilde{Z}\right) = \frac{\partial}{\partial x_j}\left[\bar{\rho}(D + D^t)\frac{\partial \tilde{Z}}{\partial x_j}\right] + \overline{\Gamma} \qquad (12)$$

with D and D^t respectively the mass diffusion coefficient and the turbulent mass diffusion coefficient. They are expressed as:

$$D = \frac{\nu}{\mathrm{Sc}} \qquad (13)$$

$$D^t = \frac{\nu^t}{\mathrm{Sc}^t} \qquad (14)$$

where Sc is the Schmidt number equal to 0.75 and Sc^t is the turbulent Schmidt number equal to 0.6. The turbulent viscosity ν^t is modeled *via* the Smagorinsky model [25] with a coefficient $C_s = 0.18$. The molecular viscosity ν is computed using a Sutherland law [25] assuming the viscosity to be independant of the gas composition and close to that of the air. $\overline{\Gamma}$ is the evaporation source term closed as in [26] assuming spherical droplets with uniform temperature. It writes:

$$\overline{\Gamma} = \pi\,\overline{n}_l\,d\,\overline{\mathrm{Sh}}\,\frac{\bar{\rho}\nu}{\mathrm{Sc}}\,ln\left(1 + \overline{B}_M\right) \qquad (15)$$

with $\overline{n}_l$ the filtered droplet density and d the droplet diameter. The filtered Sherwood number $\overline{\mathrm{Sh}}$ and the filtered mass Spalding number $\overline{B}_M$ are also introduced.

1.3.2 Mixture Fraction Variance

The determination of the mixture fraction segregation factor (*Eq. 11*) requires to transport an equation for the mixture fraction variance Z_v:

$$\frac{\partial \bar{\rho}Z_v}{\partial t} + \frac{\partial}{\partial x_j}\left(\bar{\rho}\tilde{u}_j\tilde{Z}\right) = \frac{\partial}{\partial x_j}\left[\bar{\rho}(D + D^t)\frac{\partial Z_v}{\partial x_j}\right] + 2\overline{\rho}(D + D^t)\left|\frac{\partial \tilde{Z}}{\partial x_j}\right|^2 - 2\overline{\rho D\left|\frac{\partial Z}{\partial x_j}\right|^2} + \dot{S}_{Z_v} \qquad (16)$$

The variance source term due to evaporation $\dot{S}_{Z_v}$ is modeled following [27], with a coefficient $\alpha_{\dot{w}}$ set to 0.5:

$$\dot{S}_{Z_v} = 2\bar{\rho}\alpha_{\dot{w}}Z_v\left(\frac{\overline{\Gamma}}{\tilde{Z}}\right) \qquad (17)$$

Equation (16) also introduces the filtered scalar dissipation rate computed in the CFD code as:

$$\begin{aligned}\bar{\rho}\tilde{\chi} &= \overline{\rho D\left|\frac{\partial Z}{\partial x_j}\right|^2} \\ &= \bar{\rho}D\left|\frac{\partial \tilde{Z}}{\partial x_j}\right|^2 + \left(\overline{\rho D\left|\frac{\partial Z}{\partial x_j}\right|^2} - \bar{\rho}D\left|\frac{\partial \tilde{Z}}{\partial x_j}\right|^2\right) \\ &= \bar{\rho}\tilde{\chi}_{RES} + \bar{\rho}\tilde{\chi}_{SGS}\end{aligned} \qquad (18)$$

The resolved part $\tilde{\chi}_{RES}$ of the total dissipation rate is directly computed from the filtered mixture fraction fields. In order to close the subgrid scale part, a classical equilibrium hypothesis between production and dissipation [28] of the mixture fraction segregation is retained, leading to a linear relaxation of Z_v:

$$\tilde{\chi}_{SGS} = \frac{D^t}{\Delta^2}Z_v \qquad (19)$$

with Δ the characteristic size of the filter chosen equal to the cell characteristic size. The strain rate a is then computed in the CFD code from the filtered scalar dissipation rate value:

$$a = \frac{\tilde{\chi}}{\int_{Z=0}^{Z_s} F(Z)\tilde{P}(Z)dZ} \qquad (20)$$

1.3.3 Filtered Fresh Gases Temperature

In the ADF-PCM model, the approximated diffusion flames are computed for different linear temperature stratifications $T_u(Z)$ which are characterised by the temperatures of fuel and air boundary conditions. They are determined in the CFD code using transport equations for the unburnt gases $\tilde{T}_u$ at $Z = \tilde{Z}$ and the air temperature $\tilde{T}_a$ at $Z = 0$. The filtered fuel temperature $\tilde{T}_f$ is then reconstructed by linear extrapolation as shown in Figure 2.

The filtered fresh gas temperature $\tilde{T}_u$ and the filtered fresh air temperature $\tilde{T}_a$ are determined from their respective filtered enthalpy transport equations. The temperatures are deduced from the enthalpies using the

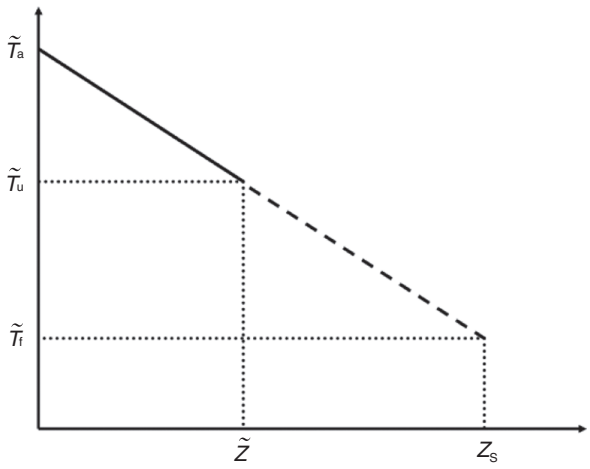

Figure 2

Scheme of the extrapolation of the fuel temperature $\tilde{T}_f$ from the fresh air $\tilde{T}_a$ and fresh gases temperature $\tilde{T}_u$.

mass fractions of the species composing either (fuel or air) stream, for which model transport equations are solved [29].

Concerning the fresh gas temperature, its filtered enthalpy $\tilde{H}_u$ is transported as:

$$\frac{\partial \bar{\rho}\tilde{H}_u}{\partial t} + \frac{\partial}{\partial x_j}\left(\bar{\rho}\tilde{u}_j\tilde{H}_u\right) = \frac{\partial}{\partial x_j}\left[\bar{\rho}\left(\frac{\nu}{\mathrm{Pr}} + \frac{\nu^t}{\mathrm{Pr}^t}\right)\frac{\partial \tilde{H}_u}{\partial x_j}\right] + \overline{\tau_{ij}}\frac{\partial \tilde{u}_i}{\partial x_j} + \frac{\bar{\rho}}{\rho_u}\frac{D\bar{P}}{Dt} + \overline{\Gamma}\left(\tilde{H} - \tilde{H}_u\right) + \dot{S}_{H_u} \tag{21}$$

where $\dot{S}_{H_u}$ denotes the evaporation source term modeled as:

$$\dot{S}_{H_u} = \overline{\Lambda} + \overline{\Phi} \tag{22}$$

The filtered enthalpy transfer terms by phase change $\overline{\Lambda}$ and filtered thermal conduction between liquid and gas $\overline{\Phi}$ write [26]:

$$\overline{\Lambda} = \overline{\Gamma} h_{s,F}(T_l) \tag{23}$$

$$\overline{\Phi} = \pi \overline{n}_l \, d \, \overline{\mathrm{Nu}} \, \overline{\lambda}\left(T_l - \tilde{T}\right) \tag{24}$$

In these equations, the liquid temperature T_l and the sensible enthalpy of the liquid fuel $h_{s,F}$ at the reference temperature T_l are introduced. The filtered Nusselt number $\overline{\mathrm{Nu}}$ is also introduced. Finally the Prandtl number Pr is equal to 0.75 and the turbulent Prandtl number Pr^t is equal to 0.6.

The filtered fresh air enthalpy is transported as:

$$\frac{\partial \bar{\rho}\tilde{H}_a}{\partial t} + \frac{\partial}{\partial x_j}\left(\bar{\rho}\tilde{u}_j\tilde{H}_a\right) = \frac{\partial}{\partial x_j}\left[\bar{\rho}\left(\frac{\nu}{\mathrm{Pr}} + \frac{\nu^t}{\mathrm{Pr}^t}\right)\frac{\partial \tilde{H}_a}{\partial x_j}\right] + \overline{\tau_{ij}}\frac{\partial \tilde{u}_i}{\partial x_j} + \frac{\bar{\rho}}{\rho_a}\frac{D\bar{P}}{Dt} + \overline{\Gamma}\left(\tilde{H} - \tilde{H}_a\right) + \dot{S}_{H_a} \tag{25}$$

with $\dot{S}_{H_a}$ the source term for the evaporation defined as:

$$\dot{S}_{H_a} = \overline{\Phi} \tag{26}$$

This transport equation represents a fictive unburnt state formed by air in a mixing between air and liquid fuel droplets. Conductive enthalpy exchanges due to temperature differences between liquid and gas are considered *via* the $\overline{\Phi}$ term. The specificity of this equation is its conditioning at $Z = 0$, where no evaporation occurs. As a result, this equation is similar to Equation (21) except that it does not take into account evaporation.

2 NUMERICAL SET-UP

The spray H [2,19,30] investigated by Sandia National Laboratories [17] has been simulated using the developed ADF-PCM model. It consists of liquid *n*-heptane fuel injected at high pressure into a constant volume vessel of approximately cubic shape with an edge length of 108 mm. It provides measurements in terms of liquid and gas penetration, pressure and flame lift-off based on OH chemiluminescence [2].

A pre-combustion is used to obtain pressure and temperature conditions prior to the start of injection that are close to those found in Diesel engines. For the simulated case, the pressure at Start of Injection (SOI) is 42.25 bar, the density 14.8 kg.m^{-3} and the temperature 1 000 K. The liquid *n*-heptane fuel is injected at 1500 bar and 373 K during 6.8 ms, leading to a total injected mass of 17.8 mg. Details can be found on the ECN web site [17].

The different initial compositions investigated are presented in Table 1. The presence of CO_2 and H_2O is due to the pre-combustion phase, necessary to reach Diesel conditions. As the mass fractions of these species are small, they are supposed to have negligible influence over combustion. They are not considered in the simulations and replaced by N_2. The experiment exhibits four reactive cases with different initial mass fractions of O_2. Oxygen in the initial gases is gradually replaced by N_2 in order to mimic effects of dilution by EGR [19]. Four ADF-PCM look-up tables are built, each of them representing one EGR rate. The last case with no oxygen corresponds to an inert case dedicated to the determination of liquid and gas penetration.

TABLE 1
Initial species mole fractions in the vessel at SOI

O_2	N_2	% EGR	CO_2	H_2O
0.21	0.6933	0	0.0611	0.0356
0.15	0.7515	28.57	0.0623	0.0362
0.12	0.7806	42.86	0.0628	0.0365
0.08	0.8195	61.90	0.0636	0.0369
0.00	0.8971	/	0.0652	0.0377

The discretisation of the look-up tables may have a strong influence on the results. In the present simulation, we used the discretisation shown in Table 2. In order to limit the number of points while keeping a good accuracy, the mixture fraction, the progress variable and the strain rate are non-linearly discretised.

The LES of these five cases were achieved using the fully compressible flow solver AVBP for unstructured hybrid meshes [20] using a second order explicit Lax-Wendroff scheme [31]. Subgrid scale turbulence is modeled with the Smagorinsky model [25] using a constant coefficient $C_s = 0.18$.

The description of the gaseous phase is based on spatially filtered Navier Stokes equations. It introduces transport equations for the momentum conservation as well as the species and the energy. The liquid spray is described using a Mesoscopic Eulerian Formalism (MEF) initially developed by Fevrier *et al.* [32] and adapted for piston engine conditions by Martinez *et al.* [33]. It requires introducing conservation equations for the droplets density, the volume fraction, the momentum, the sensible enthalpy and the uncorrelated energy resulting from the mesoscopic formalism. As MEF is only valid in regions of small liquid volume fractions, the DITurBC (Downstream Inflow Turbulent Boundary Condition) model is used. It consists in displacing the injection boundary condition downstream from the nozzle exit where the liquid volume fraction is small. Liquid and gas velocities, liquid and gas mass fractions and droplets distribution imposed on the displaced boundary conditions are determined using correlation detailed in [33].

Figure 3 displays a cut plane of the mesh used for these simulations. The mesh is composed of 22.1 million tetrahedral cells with a characteristic size of 60 µm close to the DITurBC inflow plane which gradually increases up to 600 µm at the end of the refined area. The mesh outside the cone is coarse in order to limit the overall mesh size. In this figure, the fuel mixture mass fraction is displayed. The fuel mass fraction goes up to around

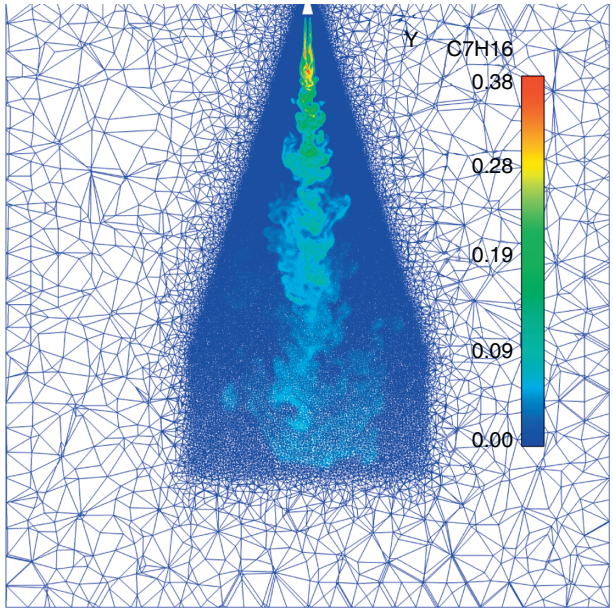

Figure 3

Computational mesh in a cut plane through the injector in which the fuel mixture fraction at 2.5 ms is displayed.

TABLE 2
Look-up table discretisation for each input variable of the ADF-PCM model

Input variable	Number of discretisation points	Range
Progress variable $\tilde{c}$	41	0-1
Mixture fraction $\tilde{Z}$	24	0-0.42
Mixture fraction segregation S_z	6	0-1
Air temperature $\tilde{T}_a$	4	700-1 000 K
Fuel temperature $\tilde{T}_f$	4	400-1 000 K
Strain rate a	11	0-8 000 s^{-1}

0.38, which is still far from Z_s chosen equal to 0.5 and below the maximum filtered mixture fraction tabulated equal to 0.42 (*Tab. 2*).

The computation of 1 ms of physical time required 9 h on 120 processors on the CCRT Titane cluster. It reaches 23 h on 400 processors for a reactive case, mainly because of the additional transport equations (for ADF-PCM model and additional species) and the time step limitation due to the combustion.

3 RESULTS AND DISCUSSION

3.1 Spray Formation

The validation of the LES prediction of the spray is performed by comparing liquid and gas penetrations with experimental findings for the non-reactive case (0% of O_2). This is achieved by following in time the evolution of the smallest axial distance from the injector outlet at which a specific variable reaches a threshold value. The threshold values used to post-process the LES are those proposed by the ECN group: a liquid volume fraction $\alpha_l = 0.0015$ for liquid penetration and a mixture fraction $Z = 0.001$ for gas penetration.

Figure 4 shows the temporal evolution of liquid and gas penetrations. Numerical and experimental liquid penetrations reach very fast a nearly constant value which is overestimated by the LES compared to the experimental one. Even so, the LES predicted liquid penetration is lower than the minimal LOL value observed which should limit the possible influence of liquid on combustion. The gas phase penetration is accurately reproduced with a small under-estimation after 1.5 ms.

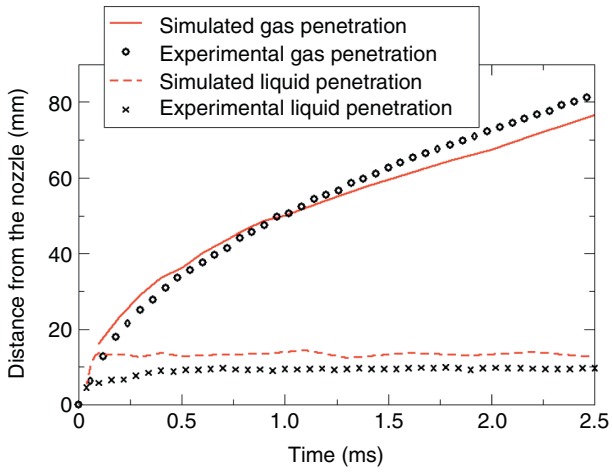

Figure 4

Temporal evolution of the liquid and gas penetrations for simulation and experiment.

3.2 Reference Case Without EGR

Figure 5 presents the evolution of the chamber pressure variation (on the left) and the HRR (on the right). The latter is deduced from the former using integral thermodynamic relations. Before $t = 0.380$ ms, almost no heat release is visible, as the spray is forming, creating by evaporation and mixing a premixture in which chemical reaction can start. After this induction phase, the auto-ignition of the so formed pre-mixture eventually leads after $t = 0.380$ ms to a non-zero combustion heat release, and to an increase of pressure. The HRR curve exhibits a strong peak until $t = 0.500$ ms, as a result of the burning of the premixture formed in the induction phase. It is consumed fast in what is generally called the premixed phase of Diesel combustion. After $t = 0.500$ ms the HRR reaches an almost constant value, leading to a linear increase of pressure with time. This phase corresponds to the non-premixed phase of Diesel combustion. This HRR profile is typical of Diesel combustion [18]. The temporal description of the combustion can be spatially observed in Figure 6 showing the temperature fields for different times after SOI. The snapshot at 0.380 ms shows the first auto-ignition spots, characterised by a temperature rise. They are located in regions of lean mixture fractions ($Z \approx 0.05$) in the downstream part of the jet, which is consistent with experimental observations [18]. The combustion then rapidly propagates and reaches the leading edge of the spray 0.550 ms after the SOI. The snapshots at $t = 1.0$ ms and 2.5 ms correspond to the non-premixed phase characterised by an almost constant HRR. The flame is anchored at a quasi-fixed axial position called the LOL. It is defined as the minimum axial location for which the temperature rise reaches half of the maximal temperature rise in the domain [12]. This temperature T_{lift} writes:

$$T_{lift} = \frac{T_{init} + T_{max}}{2} \tag{27}$$

where T_{init} is the temperature of the ambient gas before injection and T_{max} is the maximal temperature in the domain. The time evolution of the LOL is presented in Figure 7. It confirms that the combustion starts downstream in the spray and rapidly propagates upstream towards the injector until it stabilises. The experimentally observed stable LOL is accurately reproduced by the present LES.

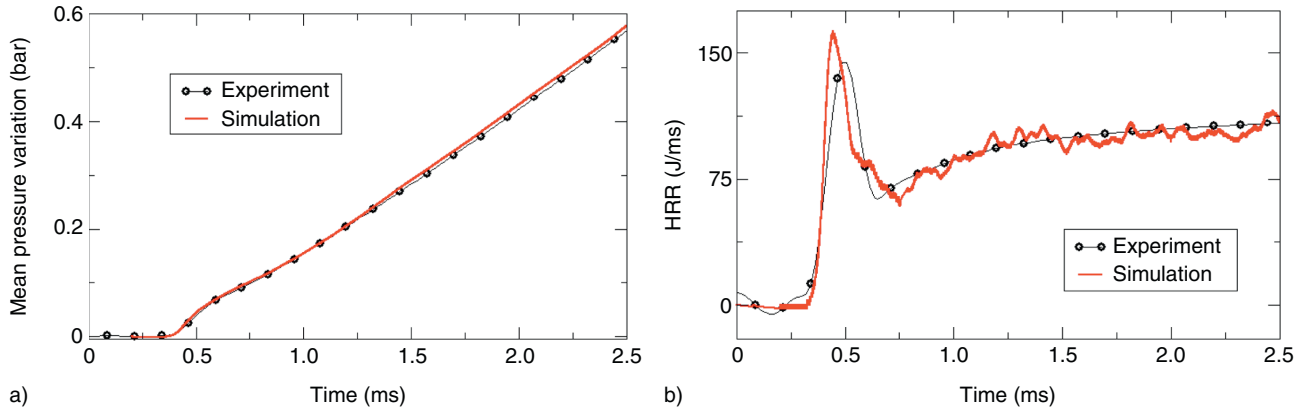

Figure 5

Temporal evolution of the mean pressure variation a) and the HRR b) for the 0% EGR experiment and simulation.

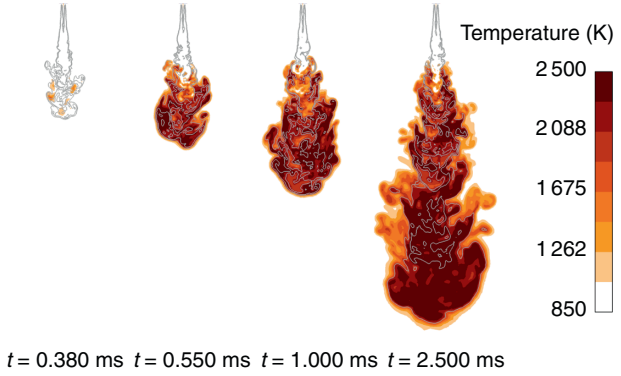

Figure 6

Temperature fields at four different times after SOI for the configuration with 0% EGR. The grey lines represent equivalence ratio isolines at 0.5, 1 and 2.

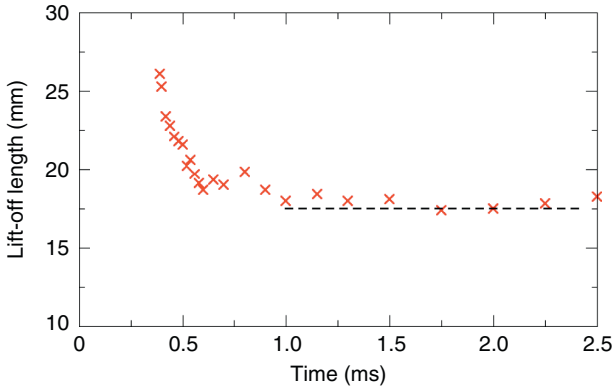

Figure 7

Temporal evolution of the LOL for the LES of the 0% EGR case. The dashed line represents the experimental stabilised LOL value.

3.3 Predicting the Impact of Increasing EGR Rate

Figure 8 compares experimental and simulated pressure rise and HRR against time for the four studied EGR rates. The HRR peak during the premixed phase decreases with increasing EGR rate, as a direct consequence of the slower chemistry resulting from O_2 depletion [1]. Increasing the EGR rate is found to have a negligible effect on the constant HRR level reached in the non-premixed phase, which remains the same for all studied EGR rates. This confirms the view presented in [19] that in the stabilised diffusion combustion phase in which the flame is anchored at the stabilized LOL, lowering the O_2 mass fraction in the initial fresh mixture is compensated by an increased LOL that increases the mixing time prior to combustion. As a result, both effects cancel each other. For all the EGR cases except the highest one, the ADF-PCM model accurately predicts the magnitude of the HRR premixed peak as well as the HRR plateau. Nevertheless the auto-ignition delays and the time occurrence of the HRR premixed peak are increasingly under-estimated with increasing EGR rates. It results in a correct reproduction of the experimental pressure curve for low EGR rates which deteriorates for high EGR rate.

The auto-ignition delay, defined as the time to reach a mean pressure rise of 1% of the mean pressure rise at 2.5 ms, is presented in Figure 9 as a function of the EGR rate. The value predicted by the present LES increases with EGR, reproducing the experimentally observed trend. However the LES increasingly underpredicts experimental values as the EGR rate is increased.

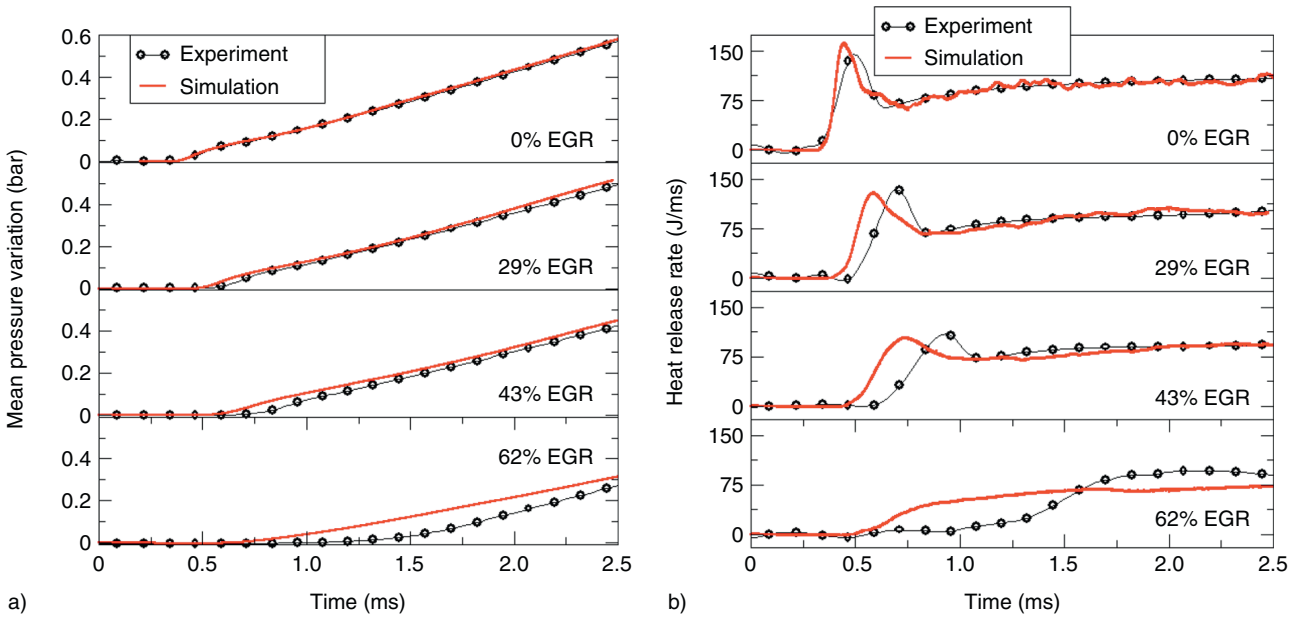

Figure 8

Temporal evolution of a) the mean chamber pressure and b) the HRR in the experiment and simulation for the four EGR rates.

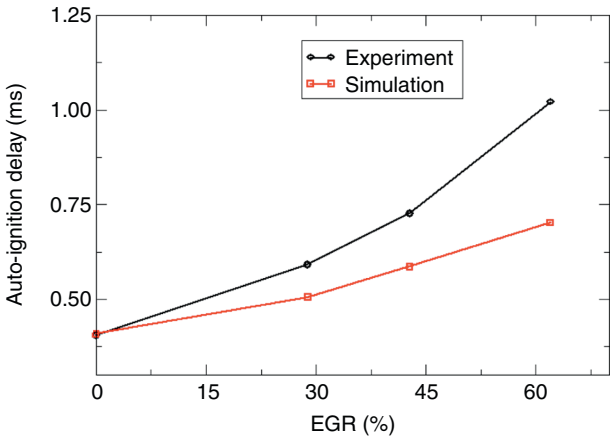

Figure 9

Auto-ignition delay as a function of the EGR rate.

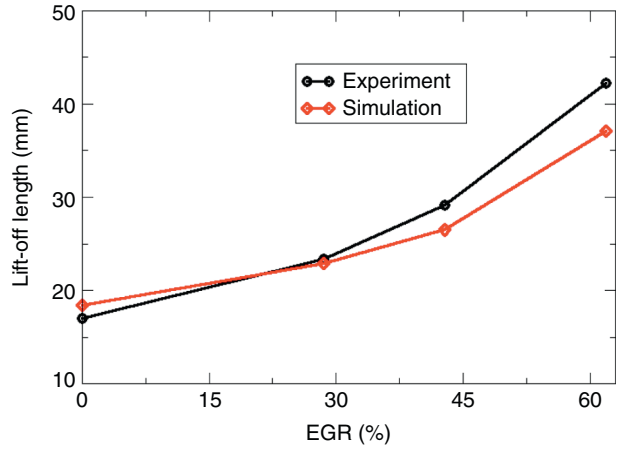

Figure 10

Evolution of the LOL as a function of the EGR rate.

Figure 10 compares numerical and experimental LOL as a function of the EGR rate. The ADF-PCM model qualitatively reproduces the effect of the EGR to increase the LOL. Predictions show good agreement for cases without or with moderate EGR rates. For the highest EGR rates however, the LOL is under-estimated.

LES successfully predicts combustion for cases with no or medium EGR rates but its accuracy decreases with increasing EGR, especially for cases with EGR rates superior to 43%. This may be related to the chemical scheme which has not been validated for oxygen mass fraction under 0.17, which in the present case would correspond to 19% of EGR. Another explanation concerns the mesh resolution. With higher EGR, the auto-ignition occurs farther from the injector nozzle, in coarser regions. Finally, the flamelet hypothesis might be blamed as the addition of EGR decreases reaction rates magnitude and therefore impacts the Damkoler number.

CONCLUSION

A LES formulation of the ADF-PCM turbulent combustion model is based on auto-igniting strained diffusion flamelets. It was coupled to an Eulerian mesoscopic formalism to be able to study liquid spray combustion. The models were implemented into the AVBP flow solver and applied to the LES of the spray H experiment from Sandia national laboratories [17]. The chemistry of the liquid *n*-heptane that is injected into a constant volume chamber under Diesel like conditions was tabulated using the Seiser [24] semi-detailed scheme containing 1 540 reactions among 160 species. In the MEF for the liquid spray, the zone close to the injector was modeled using the DITurBC approach [33].

For the reference case with no EGR, the reproduction of experimental findings by the presented LES was very accurate, with a very good reproduction of the experimentally observed mean chamber pressure evolution, HRR, auto-ignition delay and LOL. The impact of increasing the EGR rate was qualitatively reproduced, with an increase of the auto-ignition delay and of the LOL, while preserving an identical HRR once the flame has reached its stable position. However the quantitative prediction deteriorates as EGR rate is increased, with an increasing under-estimation of the auto-ignition delay and LOL with increasing EGR. This is particularly true for the highest studied EGR rate of 62%, for which the LES predicts a too fast combustion compared to the experimental findings. The Seiser chemical scheme might be blamed for this poor reproduction of the impact of increasing EGR rate as it has not been validated for low O_2 concentrations (*i.e.* high EGR rates). Other possible explanations concern the mesh refinement which is coarser far from the nozzle where high EGR cases auto-ignites and the validity of the flamelet approach, as EGR decreases the reaction rates magnitude. This will be the subject of future work.

ACKNOWLEDGMENTS

This work was granted access to the HPC resources of CCRT under the allocation 2012-026139 made by GENCI (Grand Equipement National de Calcul Intensif).

REFERENCES

1 Idicheria C., Pickett L. (2007) Eeffect of EGR on Diesel premixed burn equivalence ratios, *Proceedings of the Combustion Institute* **31**, 2931-2938.

2 Siebers D., Higgins B. (2001) Flame lift-off on direct-injection diesel sprays under quiescent conditions, *SAE Paper* 2001-01-0530.

3 Novella R., Garcia A., Pastor J.M., Domenech V. (2010) The role of detailed chemical kinetics on CFD Diesel spray ignition and combustion modelling, *Math. Comput. Model.* **54**, 1706-1719.

4 Venugopal R., Abraham J. (2007) A numerical investigation of flame lift-off in Diesel jets, *Combust. Sci. Technol.* **179**, 12, 2599-2618.

5 Gopalakrishnan V., Abrahams J. (2002) An investigation of ignition behaviour in Diesel sprays, *Proceedings of the Combustion Institute* **29**, 641-646.

6 Pitsch H., Barths H., Peters N. (1996) Three-dimensional modeling of NO_x and soot formation in DI-Diesel engines using detailed chemistry based on the interactive flamelet approach, *SAE Paper* 962057.

7 Tap F., Veynante D. (2004) Simulation of flame lift-off on a Diesel jet using a generalized flame surface density modelling approach, *Proc. Combust. Inst.* **30**, 919-926.

8 Azimov U., Kim K.S., Bae C. (2010) Modeling of flame lift-off length in Diesel low-temperature combustion with multidimensional CFD based on the flame surface density and extinction concepts, *Combust. Theory Model.* **14**, 155-175.

9 Colin O., Benkenida A. (2004) The 3-Zones Extended Coherent Flame Model (ECFM3Z) for computing premixed/diffusion combustion, *Oil Gas Sci. Technol.* **59**, 6, 593-609.

10 Hu B., Rutland C., Shethaji T.A. (2008) Combustion Modeling of Conventionnal Diesel-type and HCCI-type Diesel Combustion with Large Eddy Simulation, *SAE Paper* 2008-01-0958.

11 Seo J., Lee D., Huh K.Y., Chung J. (2010) Combustion Simulation of a Diesel Engine in the pHCCI Mode with Split Injections by the Spatially Integrated CMC Model, *Combust. Sci. Technol.* **182**, 9, 1241-1260.

12 Bekdemir C., Somers L.M.T., de Goey L.P.H., Tillou J., Angelberger C. (2013) Predicting Diesel combustion characteristics with Large-Eddy Simulations including tabulated chemical kinetics, *Proceedings of the Combustion Institute*, **34**, 2, 3067-3074.

13 Bekdemir C., Rijk E., Somers L., de Goey L., Albrecht B. (2010) On the application of the flamelet generated manifold (FGM) approach to the simulation of an igniting Diesel spray, *SAE Paper* 2010-01-0358.

14 Michel J.-B., Colin O., Veynante D. (2008) Modeling ignition and chemical structure of partially premixed turbulent flames using tabulated chemistry, *Combust. Flame*. **152**, 80-99.

15 Michel J.-B., Colin O., Angelberger C., Veynante D. (2009) Using the tabulated diffusion flamelet model ADF-PCM for simulating a lifted methane-air jet flame, *Combust. Flame*. **156**, 1318-1331.

16 Michel J.-B., Colin O., Veynante D. (2009) Comparison of differing formulations of the PCM model by their application to the simulation of an auto-igniting H_2/air jets, *Flow Turbul. Combust.* **83**, 33-60.

17 Sandia national laboratories, Engine Combustion Network (ECN), URL http://www.sandia.gov/ecn.

18 Pickett L., Siebers D., Idicheria C. (2005) Relationship Between Ignition Processes and the Lift-Off Length of Diesel Fuel Jets, *SAE Paper* 2005-01-3843.

19 Siebers D., Higgins B., Pickett L. (2002) Flame Lift-Off on Direct-Injection Diesel Fuel Jets: Oxygen Concentration Effects, *SAE Paper* 2002-01-0890.

20 Moureau V., Lartigue G., Sommerer Y., Angelberger C., Colin O., Poinsot T. (2005) High-order methods for DNS and LES of compressible multi-component reacting flows on fixed and moving grids, *J. Comput. Phys.* **202**, 2, 710-736.

21 Peters N. (1985) Numerical and asymptotic analysis of systematically reduced reaction schemes for hydrocarbon flames, in Larrouturou B., Glowinsky R., Temam R. (eds), *Numerical simulation of combustion phenomena*, Volume **241**, pp. 90-109, Springer-Verlag, Berlin.

22 Fiorina B., Baron R., Gicquel O., Thevenin D., Carpentier S., Darabiha N. (2003) Modelling non-adiabatic partially premixed flames using flame-prolongation of ILDM, *Combust. Theory Model.* **7**, 449-470.

23 Peters N. (2000) *Turbulent combustion*, Cambridge University Press.

24 Seiser R., Pitsch H., Seshadri K., Pitz W.J., Curran H.J. (2000) Extinction and autoignition of *n*-heptane in counterflow configuration, *Symposium (International) on Combustion* **28**, 2029-2037.

25 Smagorinsky J. (1963) General circulation experiments with the primitive equations. I: The basic experiment, *Monthly Weather Rev.* **91**, 3, 99-164.

26 Spalding D.B. (1953) The combustion of liquid fuels, *Proc. Combust. Inst.* **11**, 847-863.

27 Pera C., Réveillon J., Vervisch L., Domingo P. (2006) Modeling subgris scale mixture fraction variance in les of evaporating spray, *Combust. Flame* **146**, 635-648.

28 Pierce C.D., Moin P. (1998) A dynamic model for subgrid scale variance and dissipation rate of a conserved scalar, *Phys. Fluids* **10**, 12, 3041-3044.

29 Jay S., Colin C. (2011) A variable volume approach of tabulated detailed chemistry and its applications to multidimensional engine simulations, *Proceedings of the Combustion Institute* **33**, 3065-3072.

30 Idicheria C., Pickett L. (2007) Quantitative Mixing Measurements in a Vaporizing Diesel Spray by Rayleigh Imaging, *SAE Paper* 2007-01-0647.

31 Lax P.D., Wendroff B. (1960) Systems of conservation laws, *Commun. Pure Appl. Math.* **13**, 217-237.

32 Fevrier P., Simonin O., Squires K. (2005) Partitioning of Particle Velocities in Gas-Solid Turbulent Flows into a Continuous Field and a Spatially Uncorrelated Random Distribution: Theoretical Formalism and Numerical Study, *J. Fluid Mech.* **533**, 1-46.

33 Martinez L., Benkenida A., Cuenot B. (2010) A model for the injection boundary conditions in the context of 3D Simulation of Diesel Spray: Methodology and Validation, *Fuel* **89**, 1, 219-228.

Manuscript accepted in April 2013
Published online in October 2013